Magnetic Resonance Imaging of regional cardiac function in the mouse

MAGMA (2004) 17: 170–178
DOI 10.1007/s10334-004-0082-4

RESEARCH ARTICLE

E. Heijman
G. J. Strijkers
J. Habets
B. Janssen
K. Nicolay

Magnetic resonance imaging of regional cardiac function in the mouse

Received: 25 June 2004
Revised: 27 October 2004
Accepted: 29 October 2004
Published online: 20 December 2004

E. Heijman (✉) · G. J. Strijkers
J. Habets · K. Nicolay
Biomedical NMR, Department of Biomedical Engineering,
Eindhoven University of Technology,
Eindhoven, The Netherlands
E-mail: E.Heijman@tue.nl

B. Janssen
Department of Pharmacology and Toxicology, Cardiovascular Research Institute Maastricht,
Maastricht University, Maastricht,
The Netherlands

Abstract In this paper we introduce an improved harmonic phase (HARP) analysis for complementary spatial modulation of magnetization (CSPAMM) tagging of the mouse left ventricular wall, which enables the determination of regional displacement fields with the same resolution as the corresponding CINE anatomical images. CINE MRI was used to measure global function, such as the ejection fraction. The method was tested on two healthy mouse hearts and two mouse hearts with a myocardial infarction, which was induced by a ligation of the left anterior descending coronary artery. We show that the regional displacement fields can be determined. The mean circumferential strain for the left ventricular wall of one of the healthy mice was -0.09 ± 0.04 (mean $\pm$ standard deviation), while for one of the infarcted mouse hearts strains of -0.02 ± 0.02 and -0.10 ± 0.03 were found in the infarcted and remote regions, respectively.

Keywords MRI · CINE · Tagging · CSPAMM · HARP · Mouse Heart · Ejection fraction · Circumferential strain

Introduction

Myocardial infarction following cardiovascular disease is one of the major causes of death in western societies [1,2]. To improve the diagnostics and the evaluation of treatment of these diseases there is a great need for noninvasive, high-resolution imaging techniques. Magnetic resonance imaging (MRI) offers an extensive set of tools to assess both the global and local morphology and function of the heart in a noninvasive manner [3] and therefore plays an increasingly important role in the clinical management of cardiovascular disease and in basic research on disease etiology and therapeutic options.

Global functional indices of the heart, e.g., myocardial mass, end-diastolic volume, end-systolic volume and ejection fraction, can be measured using CINE MRI [4–7]. Regional tissue viability can be assessed with perfusion MR, e.g., using arterial spin labeling techniques [8], or from the delayed enhancement effect following gadolinium diethylenetriamine penta-acetic acid (Gd-DTPA) injection [9]. Phase velocity [10] and tagging techniques [11–14] are able to measure local wall motion and muscle fiber shortening, which provide important insights into local tissue function. The metabolic state of the heart tissue can be determined using ^{31}P-, ^{13}C-, or ^{23}Na magnetic resonance spectroscopy (MRS) [15–17], or by MRI measurements of the local influx of Mn^{2+}, which acts as an MRI contrast agent and can be considered a calcium analogue [18].

In vivo studies in animal models are indispensable to gain an improved understanding of the pathophysiological processes leading to myocardial infarction and to develop diagnostic tools as well as therapeutic interventions. In recent years the mouse has become the animal of choice in studies of many aspects of cardiovascular diseases, which is largely due to the large number of

transgenic and knockout mice that has become available. The significant added value of MRI for studying murine models of cardiovascular disease processes, including atherosclerosis [19–23], cardiac hypertrophy [24], and myocardial infarction [25–30], is well established.

In this paper we will present global and regional MRI measurements of left ventricle (LV) cardiac function of healthy mice and mice with a left anterior descending (LAD) coronary artery occlusion, using CINE imaging and MRI tagging. In a number of previous studies it was argued that velocity encoding is more suitable for determining regional contractility of the mouse heart than MRI tagging, because of superior resolution and the possibility to measure three-dimensional displacements [10, 31–34]. However, in this paper we demonstrate that the use of MRI tagging based on the CSPAMM technique, in combination with the harmonic phase (HARP) analysis method [35, 36], yields accurate information on regional mouse cardiac function with the same spatial resolution as the parent magnitude images.

Materials and methods

Mouse preparation

Four FVB mice (age, 18–20 weeks; weight, 20–23 g) were examined. In two mice myocardial infarction was induced by ligating the left anterior descending (LAD) coronary artery four days before the examination, using published procedures [37].

For MRI studies, the mice were first sedated in an induction chamber by exposure to 3 vol% isoflurane in medical air at a flow rate of 0.4 l/min. When the respiration rate was slowed down to approximately $1.4\,s^{-1}$ and the toe-pinch reflex was absent, the mice were transferred to a home-built support unit. A mask, which consisted of two concentric Perspex tubes, was used to supply anesthesia gas. The inner tube delivered the isoflurane (1.5 vol% in medical air; flow rate, 0.4 l/min), while the outer tube removed the excess gasses. To keep the body temperature constant, the mouse was positioned on a Perspex pad that was circulated with heated water. The mice were positioned supine on the warming pad with their head loosely fixed in the inner anesthesia tube.

For electrocardiogram (ECG) monitoring and triggering ultrasound gel (Parker Laboratories, Fairfield, NJ, USA) was put on the front paws to achieve a good electric conductivity between the animal and the ECG unit (combined ECG, respiration, and temperature monitoring unit from Rapid Biomedical, Würzburg, Germany). The paws were then fixed on copper ECG electrodes with the use of medical tape.

During the examination the respiration rate was continuously measured with a balloon pressure sensor connected to the ECG unit. The isoflurane concentration was adjusted to maintain the respiration rate within the range of $1.0–1.6\,s^{-1}$. A rectal temperature sensor (Pt100) was connected to the ECG unit and used to monitor the core temperature. The ECG, respiratory and temperature signals were continuously recorded from the ECG unit by a data acquisition PC board (National Instruments model PCI-6013, Austin, TX, USA).

The Animal Care Committee of Maastricht University (Maastricht, the Netherlands) approved the experimental protocol.

MRI protocols

The examinations were performed with a 6.3-Tesla horizontal-bore MR magnet (Oxford Instruments Superconductivity, Eynsham, Oxon, England) interfaced to a Varian (Varian, Palo Alto, CA, USA) VXR-S MR Imaging console (VNMR software 6.1B). The scanner was equipped with a Magnex gradient system (inner diameter, 9.5 cm; maximal gradient strength, 380 mT/m; rise time to full amplitude, 150 μs). A quadrature-driven birdcage coil (Rapid Biomedical, Würzburg, Germany) with an inner diameter of 3.2 cm was used for RF transmission and signal reception.

All MRI scans were collected with the use of a CINE gradient-spoiled gradient echo sequence with the following parameters: Gaussian-shaped RF pulse, 400 μs; flip angle, 30°; repetition time 10 ms; echo time, 1.3 ms; acquisition window, 1.28 ms; field of view, $2.56 \times 2.56\,cm^2$; matrix, 128×128; in-plane resolution, 200 μm; slice thickness, 1 mm; number of averages, 16. MRI scans started immediately at the up-slope of the ECG trigger pulse. The heart cycle was sampled with 10–12 images.

At the start of each examination several scout images were made in the transverse plane and the long-axis plane of the left ventricle to determine the orientation of the short-axis. The location of the central short-axis slice was planned halfway between the apex and base. Global cardiac function was next measured with a single-slice short-axis CINE sequence. By alternatingly scanning a slice above and below the central slice, the whole heart was covered within seven slices.

Tagged MR images were measured to determine the circumferential strain as a regional cardiac function parameter. For tagging, the imaging sequence described above was preceded by a complementary spatial modulation of magnetization (CSPAMM) [38] preparation (Fig. 1). The CSPAMM consisted of two Gaussian RF pulses, with a flip angle of 45° each and pulse width of 200 μs. A maximum total flip angle of 90° was chosen to simplify the analyses of the CSPAMM images. The transversal phase of the last RF pulse was either 0° or 180°, which inverted the longitudinal modulation of the tag lines.

The wavelength and the orientation of the tag lines were defined by a 200 μs gradient blip between the two RF pulses. After the second RF pulse the transversal magnetization was dephased by a crusher gradient. The total duration of the CSPAMM tagging preparation was 1 ms. The wavelength of the tag lines was 6 pixels. The tag lines were imaged with a reduced matrix of 32 k-lines in the phase-encoding direction to reduce scan time. This can be done at no cost to the resolution, since for the tagging the resolution is determined by the number of points in the read-out direction. The read-out direction was sampled with 128 points and was positioned perpendicular to the tag lines. The total MR

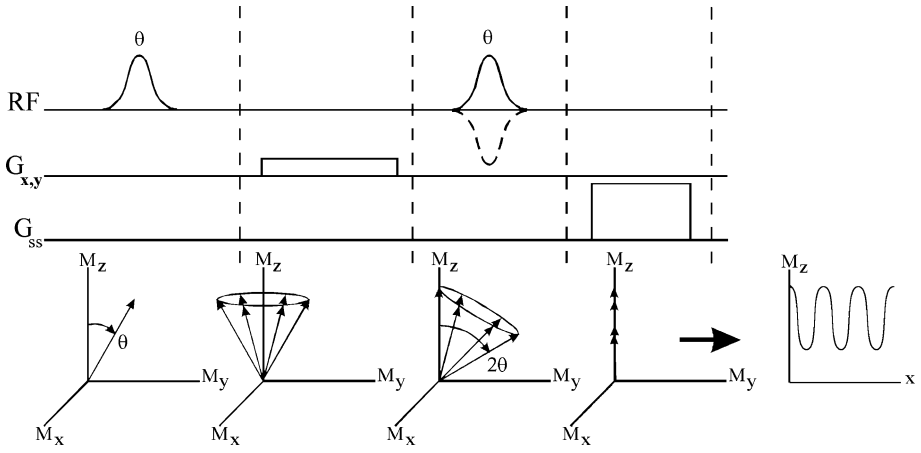

Fig. 1 The complementary spatial modulation of magnetization (CSPAMM) tagging sequence. For tagging in the *x*- or *y*-direction, a pair of RF pulses (flip angle θ) separated by a tagging gradient (G_x or G_y, respectively) generates a modulation of the longitudinal magnetization (M_z) along the *x*-axis or *y*-axis. A crusher gradient (G_{ss}) is added to spoil the transversal magnetization (M_x, M_y). To obtain two complementary tagging grids, the transversal phase of the second RF pulse is either 0° or 180°

tagging acquisition consisted of five different image acquisitions. First an anatomical image was made, which was used for segmentation of the left ventricular wall. This was followed by two CSPAMM acquisitions with horizontal and vertical tag lines, respectively. Each CSPAMM acquisition comprised two acquisitions, in which the transversal phase of the second RF pulse in the CSPAMM preparation was either 0° or 180° (Fig. 1). The total MR tagging acquisition time, for one slice, was 1 h. Three short-axis slices were measured.

Analysis of the CINE images

The global myocardial functional parameters end-diastolic (EDV) and end-systolic volumes (ESV) were determined by counting the pixels within the left ventricular cavity for all slices in the same cardiac phase. These numbers were tabulated and multiplied by the voxel area ($4{\cdot}10^{-2}$ mm^2). Summation of all the slices in the same cardiac phase and multiplication by the 1-mm slice thickness resulted in the heart volume through the cardiac cycle. The end-diastolic and end-systolic heart phases were assumed to correspond to the CINE frames with the maximal and minimal left ventricular cavity volume, respectively.

A threshold algorithm was used to create a binary image of the left ventricular cavity after the left ventricular wall was first selected as a region of interest. Because of the inhomogeneities of the RF coil and the transient state of the longitudinal magnetization, the signal intensities of the blood and myocardial wall varied for different slice positions and heart phases. All the images were therefore normalized to the intensity of the dorsal muscle to be able to apply the same threshold value for all slices. Pixels in the normalized images that were located within the left ventricular cavity or adjacent to the ventricular wall and that had a low intensity due to fast flowing blood were included in the binary.

The left ventricular wall volume was determined according to the method of Franco et al. [39]. The circumference of the left ventricular cavity, the endocardial border, was automatically determined using the threshold algorithm described above. Because of the low contrast between the myocardial wall and the chest wall, the epicardial border was segmented manually. Multiplying the left ventricular wall volume by 1.05 g/cm^3 [40] gave the left ventricular mass. The left ventricular mass was calculated for all heart phases.

The following parameters were calculated from the above measured EDV, ESV and left ventricular wall volume: stroke volume, ejection fraction, cardiac output [41] and left ventricular mass [42]. The functional parameters EDV and ESV were also determined using a manual segmentation of the left ventricular cavity. The papillary muscles were not included in the analysis.

HARP analysis

The HARmonic Phase (HARP) analysis was based on the method described by Osman et al. [43]. First the two *k*-space data sets of the CSPAMM acquisitions with horizontal tag lines were subtracted from each other. The same was done for the acquisitions with tag lines in the vertical direction. The resulting data sets were multiplied by a bandpass filter to isolate the CSPAMM convoluted image information. The bandpass filter had a cylindrical shape with its axis on the CSPAMM frequency. The filter was rotated 90° around the centre of *k*-space for the vertically tagged images. To prevent ringing or loss of tag information, the bandwidth of the filter was chosen to be 20 pixels. Once the CSPAMM frequencies were determined for the first horizontally and vertically tagged images, the same filters were used for all the successive time frames. From these filtered *k*-space data, HARP images were obtained by inverse Fourier transformation after which the phase in every pixel was calculated.

All pixels in the left ventricular wall that had been manually selected in the first CINE anatomical image were tracked throughout the cardiac cycle. The starting coordinates of the tracked points were the pixel positions in the anatomical image. Two HARP values were obtained from the first horizontal and vertical HARP images for each tracked point. In the next time frame the HARP images were locally unwrapped in an area 1.5 times the CSPAMM wavelength. The pixel quadrant with the new point position was readily identified by matching the horizontal and vertical HARP values. Next, the new point coordinates in the new pixel quadrant were locally interpolated by

fitting two surfaces through the four points of the quadrant with the horizontal and vertical HARP values. From all the tracked points, only those which remained within the left ventricular wall, based on a segmentation of the anatomical images, were included in the analysis of the circumferential strain (Ecc).

The local strain in a tracked point was determined by taking the filtered displacement derivative in Cartesian coordinates. With these derivatives the Lagrange strain [43] was calculated. A cylindrical coordinate system of the left ventricle was defined by determining the midpoint of the left ventricular wall in the first CINE anatomical image. The circumferential strain was extracted from the transformation of the Lagrange strain from the Cartesian to the cylindrical coordinate system.

The CINE analyses, the HARP analyses and the calculation of the strains were done using Matlab 6.1 (The Mathworks Inc., Natick, MA, USA)

Results

In the first part of the study it was found that the mouse heart rate was sensitive to the body temperature. The heart rate became also unstable over time when the body temperature was not maintained around 37°C. Because of this, the mice had a relative large variation in heart rate throughout the examination: for the control animal the heart rate ranged from 520 to 600 beats/min, and for the infarct mouse from 428 to 492 beats/min. To decrease the examination time, we only used ECG triggering and turned the respiratory gating off. The results are shown in Fig. 2. Almost no artifacts due to respiratory motion were observed in the noise of the images. The total acquisition time now became 7 min for a single-slice CINE series, while amounting to circa 13 min with respiratory gating on.

The global myocardial functional parameters for the healthy mouse and infarcted mouse are shown in Table 1. The comparison of the above values is indicative of the compromised cardiac function induced by the focal infarction and corresponds to data measured in conscious mice using direct flow measurements at the ascending aorta [44].

Next, MRI tagging experiments were performed to determine regional cardiac function. To reduce the heart rate fluctuations caused by the body temperature variation during the experiments, both mice were kept at a body temperature of 37.4 ± 0.5°C. The heart rate for the healthy mouse was ranging from 467 to 477 beats/min during the whole acquisition. The infarcted mouse had a larger heart rate fluctuation of 500 to 590 beats/min.

In Fig. 3 the data of the tagging procedure is shown. In the top row the subtracted horizontal tagged CSPAMM images are represented. The image of the healthy mouse (Fig. 3a) was rotated 45° counterclockwise to have approximately the same anatomical orientation as the other two images. For the infarcted mouse heart two slices were acquired for comparison, one within the infarcted region (Fig. 3b) and one above the region (Fig. 3c). Both regions were planned on the basis of the CINE MRI images. Histology (data not shown) showed that the regions were correctly chosen, retrospectively.

The bottom row of Fig. 3 shows the calculated circumferential strains overlaid on top of the anatomical CINE images. A large difference in circumferential strain was found between the healthy (Fig. 3a) and the infarcted mouse heart (Fig. 3b), where the latter had a high circumferential strain gradient in the apical inferoseptal region. This atypical contraction pattern in this part of the myocardium was also evident from the assessment of the CINE CSPAMM images. The circumferential strain in the slice above the infarction (Fig. 3c) was higher than the values observed at a similar slice position in the healthy mouse.

Figure 4 shows a more global analysis of the strain data by separating the left ventricular wall into octants. The resulting mean circumferential strain of each octant is plotted as function of time for healthy (dotted lines), infarcted (solid lines) and remote (dashed lines) regions. For the infarcted heart octants 3–6 in the left ventricular free wall appeared hypokinetic compared to the healthy heart, while remote regions in the septum were hyperkinetic. The mean circumferential strain of the total slice through the left ventricular wall of the healthy mouse heart and the infarct slice and remote slice for the case of the infarcted mouse heart are presented in Table 2.

Discussion

The primary goal of this study was to show that MRI tagging, combined with HARP analysis, enables the detailed analysis of the regional function of the mouse heart. This was demonstrated for healthy and infarcted mouse hearts. MRI tagging was combined with CINE MRI for the assessment of global myocardial function.

For the CINE measurements respiratory gating was omitted, resulting in a major reduction of the scan time. This is favorable because it is difficult to keep the heart rate of the mouse stable over longer periods of time, especially for those mice with a myocardial infarction. Nevertheless, as can be seen in the bottom row of Fig. 2, no severe respiratory movement artifacts were introduced in comparison with, for example, those reported in Ref. [45]. However, the through and in-plane motion of the blood resulted in small artifacts in the phase-encoding direction. These artifacts can be reduced by using flow-compensated gradients [46]. We have chosen not to use additional flow compensation because this increases the echo time, which results in loss of signal in the CINE images due to the short T_2^* of the myocardium and therefore a lower signal-to-noise ratio. Moreover, the MRI tagging technique is not very sensitive to phase errors, in contrast to the velocity-encoding technique, and therefore the small artifacts

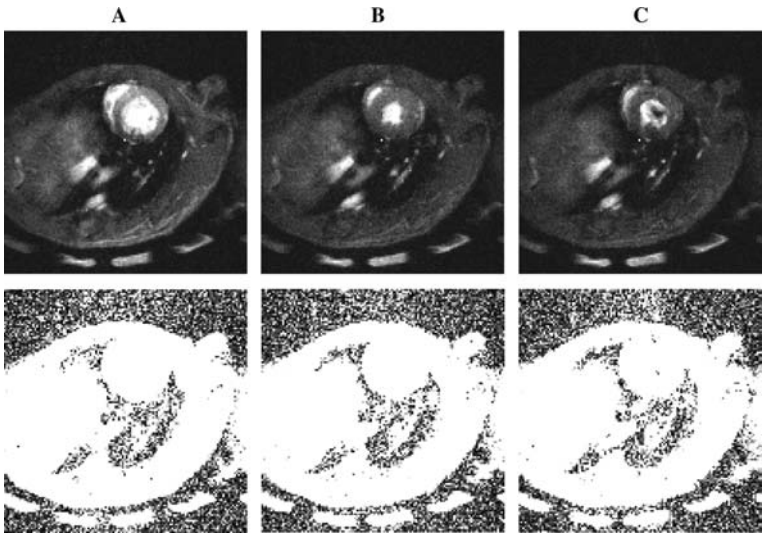

Fig. 2 (Top) Short-axis images of the left ventricle of healthy mouse heart at end-diastole (**a**), end-systole (**b**) and during rapid filling (**c**). (Bottom) The same images as the top row with decreased maximum value of the intensity range to reveal potential low-level artifacts. The phase-encoding gradient was applied in the vertical direction

Table 1 Global myocardial functional parameters from control and infarcted mouse heart as determined from short-axis CINE images. EDV: end-diastole volume; ESV: end-systole volume; SV: stroke volume; EF: ejection fraction; CO: cardiac output; LV: left ventricular

	EDV [μl]	ESV [μl]	SV [μl]	EF [-]	CO [ml/min]	LV mass [mg]†
Control	63	21	42	0.66	23.0	112±9*
Infarcted	64	38	27	0.41	12.2	149±6**

† Shown as mean ± standard deviation, for: * N=10 heart phases; ** N=12 heart phases

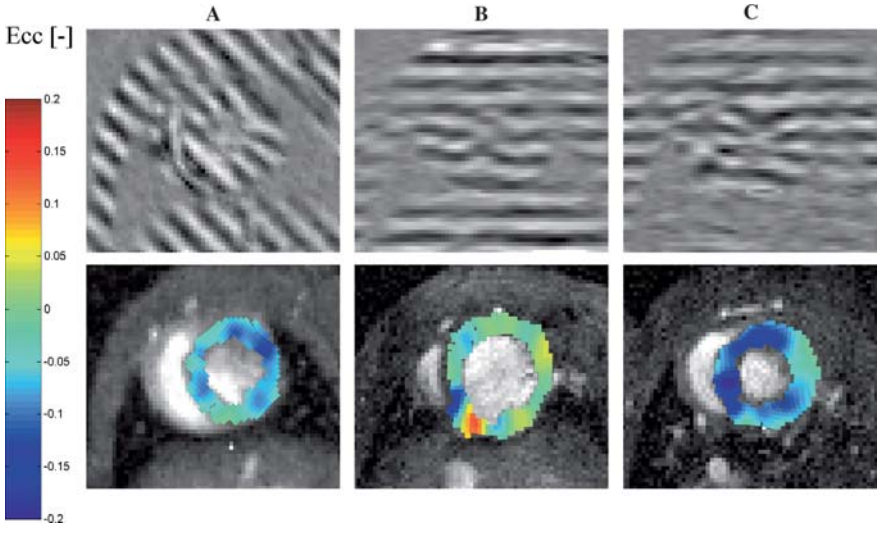

Fig. 3 The top row shows horizontally tagged CSPAMM images of a healthy mouse heart (**a**) and an infarcted mouse heart (**b**, **c**) at end-systole. Slice B was positioned through the infarct region, while slice C was located remote above the infarction. The bottom row represents the calculated circumferential strain (Ecc) in every tracked point at end-systole. The Ecc is color coded according to the colorbar on the left. The data from the healthy mouse is rotated by 45° to obtain approximately the same anatomical orientation as the other data

introduced by the flowing blood will not compromise the tagging analysis.

Because of this reduction in acquisition time it was possible to measure the left ventricular volume, using the multi-slice sequence, within a reasonable amount of time (approximately 2 h). At the location of the infarction, apical anterior, the relative difference between end-diastolic and end-systolic ventricular areas was considerably less for the mouse with myocardial infarction. This is a consequence of the impaired contractility of the myocardial wall introduced by the infarction and can also be observed in the tagging images (Fig. 3) discussed further on.

Since the in-plane spatial resolution of 200 μm is still rather coarse, the position and volume taken by the papillary muscles could not be determined with high accuracy automatically. Furthermore, the automatic segmentation method introduces some errors because of partial volume effects at the myocardial wall and the closing of the trabeculae at the end-systolic period. To assess the errors introduced in the determination of the ventricular volumes, we

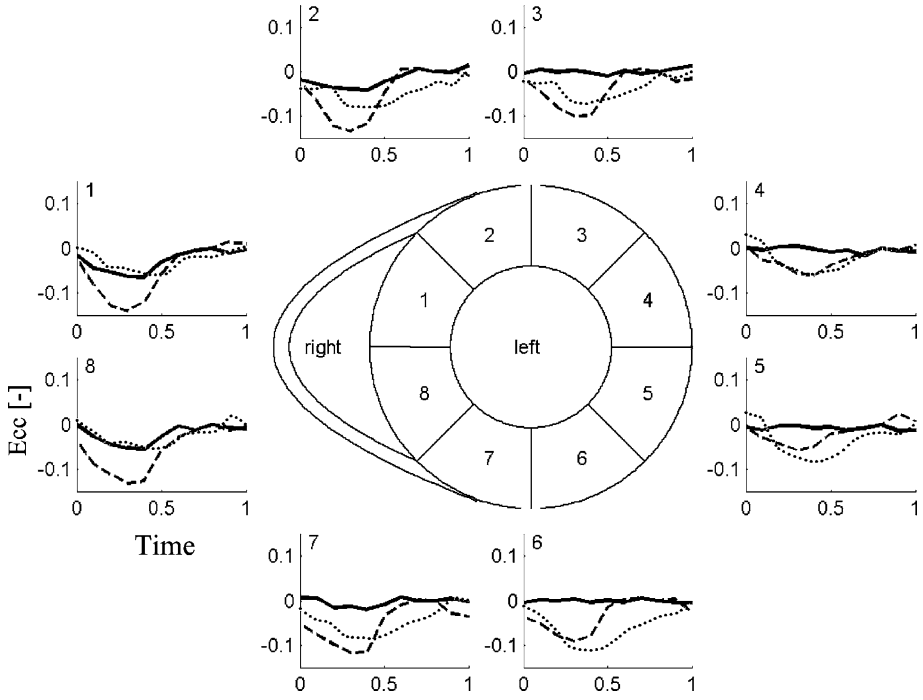

Fig. 4 Analysis of the circumferential strain (Ecc) in eight zones of the left ventricular wall as function of time in a healthy mouse (*dotted line*), and for a mouse with infarction. The solid line represents a slice positioned through the infarct region, while the dashed line represents a slice remote above the infarction. Septum, zone 1 and 8; anterior, zone 2 and 3; lateral, zone 4 and 5; posterior, zone 6 and 7. The *x*-axis denotes the time through the cardiac cycle going from 0, begin-systole, to 1, end-diastole

Table 2 Mean circumferential strain of the left ventricular wall for different regions from control and infarcted mouse heart

Region	Mean circumferential strain†
Control	-0.09 ± 0.04[a]
Infarcted:	
Infarct slice	-0.02 ± 0.02[b]
Remote slice	-0.10 ± 0.03[c]

† Shown as mean ± standard deviation, for tracked points: [a]N = 274; [b]N = 350; [c]N = 337 (N = Number of pixels)

have compared the automatic segmentation with an expert manual segmentation. In general, the manual segmentation resulted in a 15% lower ESV and EDV, because of more accurate exclusion of papillary muscles and trabeculae. The ejection fraction however remained the same for both methods. The ejection fraction values found (Table 1) are comparable with other studies of mouse ventricular function [30, 47–49].

The CSPAMM tagging images were measured with the same resolution in the read-out direction as the CINE images. A major advantage of the CSPAMM technique is that the zero-order image information in *k*-space is filtered away efficiently and automatically. This will lead to a lower error in the strain and fewer artifacts [36].

A modified HARP analysis was used to track the material points on the left ventricular wall. This method has the advantage that we obtain comparable resolutions for the CINE and the displacement images, in contrast to the method described by Atalar [50], which results in a resolution decrease of at least a factor of 4. From begin-systole to end-systole the spatial resolution of the tracked points becomes even higher than the starting resolution, because material points are allowed to move towards each other as the heart contracts.

There are several alternative MRI methods to measure regional displacements and strains in the myocardial wall, such a velocity encoding and Displacement ENcoding with Stimulated Echo (DENSE). However, velocity encoding is extremely sensitive to phase errors and needs time-consuming velocity encoding and compensation of the MRI sequence. Furthermore, this method measures velocities rather than displacements, which makes it significantly more difficult to determine regional strains. Velocity encoding has the advantage that it can be used more easily in a three-dimensional manner. DENSE [34] can also accurately measure displacements and strains with high spatial and temporal resolution. The main drawback of DENSE is a longer acquisition time due to the intrinsically lower signal-to-noise ratio.

The circumferential strains in Figs. 3 and 4 show that there was no uniform distribution of strain values over the left ventricular wall of the infarcted mouse heart. The measured mean circumferential strain of the healthy mouse heart is lower than reported in the literature [12, 34], which might be explained by differences in mouse strain. Although a detailed analysis of the regional strains in relation to the induced infarction is beyond the scope of this paper, it is noteworthy that the circumferential strain in the slice above the infarction (Fig. 3c and Fig. 4) was higher

than that in the healthy myocardial wall. This might be explained by the fact that different regions of the mouse heart are going through a process of differential remodeling and adaptation such as also observed in humans [51, 52] and canines [53]. In contrast, Epstein et al. [12] have found impairment of the remote myocardium in mice. Their study, however, differs from our study by a difference in the adaptation time following infarction, 4 days versus 1 day, and a difference in the mouse model, reperfusion versus permanent occlusion. The mean circumferential strains in the infarcted region were lower than found in other studies [12, 34]. These differences might be caused by differences in the measuring position and differences in the extent of the induced infarction. The infarcted slice (Fig. 3b) showed an area with a high strain gradient in the apical inferoseptal region. Analysis of the CINE CSPAMM images in this region showed a small compression in the upper part and a small stretching in the lower part consistent with the strain analysis. From this we conclude that the area is still active and not infarcted but has an atypical contraction pattern. The circumferential strain outside the infarcted region is within the range of previously reported values [12, 34].

Conclusions

This study demonstrates the feasibility of MRI methods to measure and quantify global and regional function of mouse hearts with myocardial infarction, using CINE and CSPAMM tagging with HARP analysis. The ejection fraction can be measured with sufficient accuracy to distinguish between healthy and infarcted mouse hearts. We have shown that MRI tagging, combined with an improved HARP analysis enables the detailed determination of regional displacements within the ventricular wall. From these displacements the circumferential strain can be calculated, providing information on local function in healthy and infarcted hearts, with a comparable resolution as the anatomical images.

Acknowledgements The authors thank Theo Arts, Peter Bovendeerd and Sander Ubbink for the Matlab code for calculating the circumferential strain and fruitful discussions. Larry de Graaf is acknowledged for technical assistance.

References

1. Ross R (1993) The pathogenesis of atherosclerosis: a perspective for the 1990s. Nature 362:801–809
2. Glass CK, Witztum JL (2001) Atherosclerosis: the road ahead. Cell 104:503–516
3. de Roos A, Kunz P, Lamb H, Kroft L, Langerak S, Doornbos J, van der WE (1999) Magnetic resonance imaging of ischemic heart disease: why cardiac magnetic resonance imaging will play a significant role in the management of patients with coronary artery disease. J Comput Assist Tomogr 23 (Suppl 1):S135-S141
4. Semelka RC, Tomei E, Wagner S, Mayo J, Caputo G, O'Sullivan M, Parmley WW, Chatterjee K, Wolfe C, Higgins CB (1990) Interstudy reproducibility of dimensional and functional measurements between cine magnetic resonance studies in the morphologically abnormal left ventricle. Am Heart J 119:1367–1373
5. Semelka RC, Tomei E, Wagner S, Mayo J, Kondo C, Suzuki J, Caputo GR, Higgins CB (1990) Normal left ventricular dimensions and function: interstudy reproducibility of measurements with cine MR imaging. Radiology 174:763–768
6. Florentine MS, Grosskreutz CL, Chang W, Hartnett JA, Dunn VD, Ehrhardt JC, Fleagle SR, Collins SM, Marcus ML, Skorton DJ (1986) Measurement of left ventricular mass in vivo using gated nuclear magnetic resonance imaging. J Am Coll Cardiol 8:107–112
7. van der Geest RJ, Reiber JH (1999) Quantification in cardiac MRI. J Magn Reson Imaging 10:602–608
8. Reeder SB, Holmes AA, McVeigh ER, Forder JR (1999) Simultaneous noninvasive determination of regional myocardial perfusion and oxygen content in rabbits: toward direct measurement of myocardial oxygen consumption at MR imaging. Radiology 212:739–747
9. Kroft LJ, de Roos A (1999) Blood pool contrast agents for cardiovascular MR imaging. J Magn Reson Imaging 10:395–403
10. Streif JU, Herold V, Szimtenings M, Lanz TE, Nahrendorf M, Wiesmann F, Rommel E, Haase A (2003) In vivo time-resolved quantitative motion mapping of the murine myocardium with phase contrast MRI. Magn Reson Med 49:315–321
11. Castillo E, Lima JA, Bluemke DA (2003) Regional myocardial function: advances in MR imaging and analysis. Radiographics 23 Spec No:S127-S140
12. Epstein FH, Yang Z, Gilson WD, Berr SS, Kramer CM, French BA (2002) MR tagging early after myocardial infarction in mice demonstrates contractile dysfunction in adjacent and remote regions. Magn Reson Med 48:399–403
13. Henson RE, Song SK, Pastorek JS, Ackerman JJ, Lorenz CH (2000) Left ventricular torsion is equal in mice and humans. Am J Physiol Heart Circ Physiol 278:H1117-H1123
14. Zhou R, Pickup S, Glickson JD, Scott CH, Ferrari VA (2003) Assessment of global and regional myocardial function in the mouse using cine and tagged MRI. Magn Reson Med 49:760–764
15. Schaefer S, Balaban RS (1993) Cardiovascular magnetic resonance spectroscopy. Kluwer, Boston, p. 230
16. Chacko VP, Aresta F, Chacko SM, Weiss RG (2000) MRI/MRS assessment of in vivo murine cardiac metabolism, morphology, and function at physiological heart rates. Am J Physiol Heart Circ Physiol 279:H2218-H2224

17. Omerovic E, Basetti M, Bollano E, Bohlooly M, Tornell J, Isgaard J, Hjalmarson A, Soussi B, Waagstein F (2000) In vivo metabolic imaging of cardiac bioenergetics in transgenic mice. Biochem Biophys Res Commun 271:222–228
18. Hu TC, Pautler RG, MacGowan GA, Koretsky AP (2001) Manganese-enhanced MRI of mouse heart during changes in inotropy. Magn Reson Med 46:884–890
19. Wiesmann F, Szimtenings M, Frydrychowicz A, Illinger R, Hunecke A, Rommel E, Neubauer S, Haase A (2003) High-resolution MRI with cardiac and respiratory gating allows for accurate in vivo atherosclerotic plaque visualization in the murine aortic arch. Magn Reson Med 50:69–74
20. Choudhury RP, Fayad ZA, Aguinaldo JG, Itskovich VV, Rong JX, Fallon JT, Fisher EA (2003) Serial, noninvasive, in vivo magnetic resonance microscopy detects the development of atherosclerosis in apolipoprotein E-deficient mice and its progression by arterial wall remodeling. J Magn Reson Imaging 17:184–189
21. Choudhury RP, Aguinaldo JG, Rong JX, Kulak JL, Kulak AR, Reis ED, Fallon JT, Fuster V, Fisher EA, Fayad ZA (2002) Atherosclerotic lesions in genetically modified mice quantified in vivo by non-invasive high-resolution magnetic resonance microscopy. Atherosclerosis 162:315–321
22. Fayad ZA, Fallon JT, Shinnar M, Wehrli S, Dansky HM, Poon M, Badimon JJ, Charlton SA, Fisher EA, Breslow JL, Fuster V (1998) Noninvasive in vivo high-resolution magnetic resonance imaging of atherosclerotic lesions in genetically engineered mice. Circulation 98:1541–1547
23. Itskovich VV, Choudhury RP, Aguinaldo JG, Fallon JT, Omerhodzic S, Fisher EA, Fayad ZA (2003) Characterization of aortic root atherosclerosis in ApoE knockout mice: high-resolution in vivo and ex vivo MRM with histological correlation. Magn Reson Med 49:381–385
24. Franco F, Dubois SK, Peshock RM, Shohet RV (1998) Magnetic resonance imaging accurately estimates LV mass in a transgenic mouse model of cardiac hypertrophy. Am J Physiol 274:H679-H683
25. Nahrendorf M, Wiesmann F, Hiller KH, Han H, Hu K, Waller C, Ruff J, Haase A, Ertl G, Bauer WR (2000) In vivo assessment of cardiac remodeling after myocardial infarction in rats by cine-magnetic resonance imaging. J Cardiovasc Magn Reson 2:171–180
26. Nahrendorf M, Wiesmann F, Hiller KH, Hu K, Waller C, Ruff J, Lanz TE, Neubauer S, Haase A, Ertl G, Bauer WR (2001) Serial cine-magnetic resonance imaging of left ventricular remodeling after myocardial infarction in rats. J Magn Reson Imaging 14:547–555
27. Nahrendorf M, Hiller KH, Hu K, Ertl G, Haase A, Bauer WR (2003) Cardiac magnetic resonance imaging in small animal models of human heart failure. Med Image Anal 7:369–375
28. Nahrendorf M, Hu K, Fraccarollo D, Hiller KH, Haase A, Bauer WR, Ertl G (2003) Time course of right ventricular remodeling in rats with experimental myocardial infarction. Am J Physiol Heart Circ Physiol 284:H241-H248
29. Waller C, Hiller KH, Kahler E, Hu K, Nahrendorf M, Voll S, Haase A, Ertl G, Bauer WR (2001) Serial magnetic resonance imaging of microvascular remodeling in the infarcted rat heart. Circulation 103:1564–1569
30. Ross AJ, Yang Z, Berr SS, Gilson WD, Petersen WC, Oshinski JN, French BA (2002) Serial MRI evaluation of cardiac structure and function in mice after reperfused myocardial infarction. Magn Reson Med 47:1158–1168
31. Markl MM, Chan FP, Alley MT, Wedding KL, Draney MT, Elkins CJ, Parker DW, Wicker R, Taylor CA, Herfkens RJ, Pelc NJ (2003) Time resolved three-dimensional phase-contrast MRI. J Magn Reson Imaging 17:499–506
32. Wedding KL, Draney MT, Herfkens RJ, Zarins CK, Taylor CA, Pelc NJ (2002) Measurement of vessel wall strain using cine phase contrast MRI. J Magn Reson Imaging 15:418–428
33. Arai AE, Gaither CC, Epstein FH, Balaban RS, Wolff SD, et al. (1999) Myocardial velocity gradient imaging by phase contrast MRI with application to regional function in myocardial ischemia. Magn Reson Med 42:98–109
34. Gilson WD, Yang Z, French BA, Epstein FH (2004) Complementary displacement-encoded MRI for constrast enhanced infarct detection and quatification of myocardial function in mice. Magn Reson Med 51:744–752
35. Ryf S, Spiegel MA, Gerber M, Boesiger P (2002) Myocardial tagging with 3D-SPAMM. J Magn Reson 16:320–325
36. Kuijer JPA, Jansen E, Marcus JT, van Rossum AC, Heethaar RM (2001) Improved harmonic phase myocardial strain maps. Magn Reson Med 46:993–999
37. Lutgens E, Daemen MJ, de Muinck ED, Debets J, Leenders P, Smits JF (1999) Chronic myocardial infarction in the mouse: cardiac structural and functional changes. Cardiovasc Res 41:586–593
38. Fischer SE, McKinnon GC, Maier SE, Boesiger P (1993) Improved myocardial tagging contrast. Magn Reson Med 30:191–200
39. Franco F, Dubois SK, Peshock RM, Shohet RV (1998) Magnetic resonance imaging accurately estimates LV mass in a transgenic mouse model of cardiac hypertrophy. Am J Physiol 274:H679-H683
40. Franco F, Dubois SK, Peshock RM, Shohet RV (1998) Magnetic resonance imaging accurately estimates LV mass in a transgenic mouse model of cardiac hypertrophy. Am J Physiol 274:H679-H683
41. Guyton AC, Hall JE (1996) Heart muscle; the heart as a pump. Textbook of medical physiology. Saunders, Philadelphia, pp. 107–119
42. Franco F, Dubois SK, Peshock RM, Shohet RV (1998) Magnetic resonance imaging accurately estimates LV mass in a transgenic mouse model of cardiac hypertrophy. Am J Physiol 274:H679-H683
43. Osman NF, Kerwin WS, McVeigh ER, Prince JL (1999) Cardiac motion tracking using CINE harmonic phase (HARP) magnetic resonance imaging. Magn Reson Med 42:1048–1060
44. Janssen BJA, Smits JFM (2002) Autonomic control of blood pressure in mice: basic physiology and effects of genetic modification. Am J Physiol Regul Integr Comp Physiol 282:R1545-R1564
45. Cassidy PJ, Schneider JE, Grieve SM, Lygate C, Neubauer S, Clarke K (2004) Assessment of motion gating strategies for mouse magnetic resonance at high magnetic field. J Magn Reson Imaging 19:229–237
46. Haacke FM, Brown RW, Thompson MR, Venkatesan R (1999) Magnetic resonance imaging: physical principles and sequence design. Wiley, New York
47. Wiesmann F, Ruff J, Hiller KH, Rommel E, Haase A, Neubauer S (2000) Development changes of cardiac function and mass assessed with MRI in neonatal, juvenile and adult mice. Am J Physiol Heart Circ Physiol 278:H652-H657
48. Chacko VP, Aresta F, Chacko SM, Weiss RG (2000) MRI/MRS assessment of in vivo murine cardiac metabolism, morphology and function at physiological heart rates. Am J Physiol Heart Circ Physiol 279: H2218-H2224

49. Wiesmann F, Frydrychowicz A, Rautenberg J, Illinger R, Rommel E, Haase A, Neubauer S (2002) Analysis of right ventricular function in healthy mice and a murine model of heart failure by in vivo MRI. Am J Physiol Heart Circ Physiol 283:H1065-H1071
50. Atalar E, McVeigh ER (1994) Optimization of tag thickness for measuring position with magnetic resonance imaging. IEEE Trans Med Im 13:152–160
51. Nieminen M, Heikkila J (1976) Echoventriculography in acute myocardial infarction. III. Clinical correlations and implication of the noninfarcted myocardium. Am J Cardiol 38:1–8
52. Rigaud M, Rocha P, Boschat J, Farcot JC, Bardet J, Bourdarias JP (1979) Regional left ventricular function assessed by contrast angiography in acute myocardial infarction. Circulation 60:130–139
53. Lew WY, Chen ZY, Guth B, Covell JW (1985) Mechanisms of augmented segment shortening in nonischemic areas during acute ischemia of the canine left ventricle. Circ Res 56:351–358